CHEMISTRY
A EUROPEAN JOURNAL

ChemPubSoc
Europe

DOI: 10.1002/chem.201301871

Design of Glycosyltransferase Inhibitors: Pyridine as a Pyrophosphate Surrogate

Shuai Wang,[a] Jose A. Cuesta-Seijo,[b] Dominique Lafont,[a] Monica M. Palcic,[b] and Sébastien Vidal*[a]

Abstract: A series of ten glycosyltransferase inhibitors has been designed and synthesized by using pyridine as a pyrophosphate surrogate. The series was prepared by conjugation of carbohydrate, pyridine, and nucleoside building blocks by using a combination of glycosylation, the Staudinger–Vilarrasa amide-bond formation, and azide–alkyne click chemistry. The compounds were evaluated as inhibitors of five metal-dependent galactosyltransferases. Crystallographic analyses of three inhibitors complexed in the active site of one of the enzymes confirmed that the pyridine moiety chelates the Mn^{2+} ion causing a slight displacement (2 Å) from its original position. The carbohydrate head group occupies a different position than in the natural uridine diphosphate (UDP)–Gal substrate with little interaction with the enzyme.

Keywords: carbohydrates · click chemistry · inhibitors · ligation · X-ray diffraction

Introduction

Glycosyltransferases[1,2] (GTs) are responsible for the formation of glycosidic bonds with high regio- and stereoselectivity. The majority of GTs utilize so-called Leloir donors[3] catalyzing the transfer of a carbohydrate from a nucleotide sugar (such as a nucleotide (di)phosphate sugar, NDP sugar) to an acceptor substrate (typically a mono- or oligosaccharide) with the concomitant release of a nucleotide diphosphate (NDP). The transfer can occur with retention or inversion of the configuration at the anomeric center of the carbohydrate transferred from the NDP sugar donor (Figure 1).

Many mammalian cell surface oligosaccharides display the sialyl Lewis x epitope, which is involved in inflammation,[4,5] fecundation,[6,7] rheumatoid arthritis,[8,9] or cancer.[10,11] Its biosynthesis requires the action of a β-1,4-galactosyltransferase (β-1,4-GalT) whose inhibition has potential biomedical applications. Pig to human xenotransplantations are limited by immune rejection due to the presence of Galα-1,3-LacNAc epitopes on animal organs. The design of α-1,3-galactosyltransferase (α-1,3-GalT) inhibitors can be applied to reduce immune rejection of xenografts.[12] Human blood group B galactosyltransferase α-1,3-GalT[13] (GTB) is an enzyme involved in the α-galactosylation of the human H-antigen to produce the blood group B oligosaccharide epitope. GTB is a well characterized model glycosyltransferase for stucture–function studies and inhibitor design strategies. Comparision with a closely related murine blood group A and B-synthesizing α-1,3-GalT/GalNAcT (AAGlyB) can be used to evaluate the inhibitor specificity.[14] α-1,4-Galactosyltransferase (α-1,4-GalT) is found in some human pathogenic bacteria. It adds a galactose resdiue to terminal lactose in lipooligosaccharides and the inhibiton of α-1,4-GalT has been suggested for the development of novel antivirulence compounds and antimicrobials.[15]

The inhibition of GTs has typically been approached through the design of donor or bi-substrate analogues by using conventional[16–20] or combinatorial[21–23] approaches, with a few examples for acceptor analogues.[24] For metal-dependent GTs of the GT-A fold, the pyrophosphate moiety of the donor interacts with cations (e.g., Mn^{2+} or Mg^{2+}) with coordination to two aspartate residues within a DXD motif (Figure 1). Several analogues of NDP sugars with modifications of the diphosphate unit have been designed, such as phosphonates,[25–29] methylenediphosphonates,[30,31] or methylpyrophosphates.[32,33] However, there is limited data reported with respect to the inhibition of their target GTs.[28,31,33–36]

The main drawback of this approach is the anionic character of the inhibitors, which precludes their entry into cells due to repulsion by the anionic phospholipid bilayer. The preparation of neutral inhibitors of GTs[14,37–46] is emerging as a promising strategy for in vivo biological applications. Because the diphosphate unit of the NDP sugars interacts with cations in metal-dependent GTs, any surrogate of this moiety should be capable of coordinating to the metal. With

[a] S. Wang, Dr. D. Lafont, Dr. S. Vidal
Institut de Chimie et Biochimie Moléculaires et Supramoléculaires
Laboratoire de Chimie Organique 2, Glycochimie, UMR 5246
CNRS and Université Claude Bernard Lyon 1
43 Boulevard du 11 Novembre 1918
6922 Villeurbanne (France)
Fax: (+33) 472-448-109
E-mail: sebastien.vidal@univ-lyon1.fr

[b] Dr. J. A. Cuesta-Seijo, Prof. M. M. Palcic
Carlsberg Laboratory, Gamle Carlsberg Vej 10
1799 Copenhagen V (Denmark)

Supporting information for this article is available on the WWW under http://dx.doi.org/10.1002/chem.201301871.

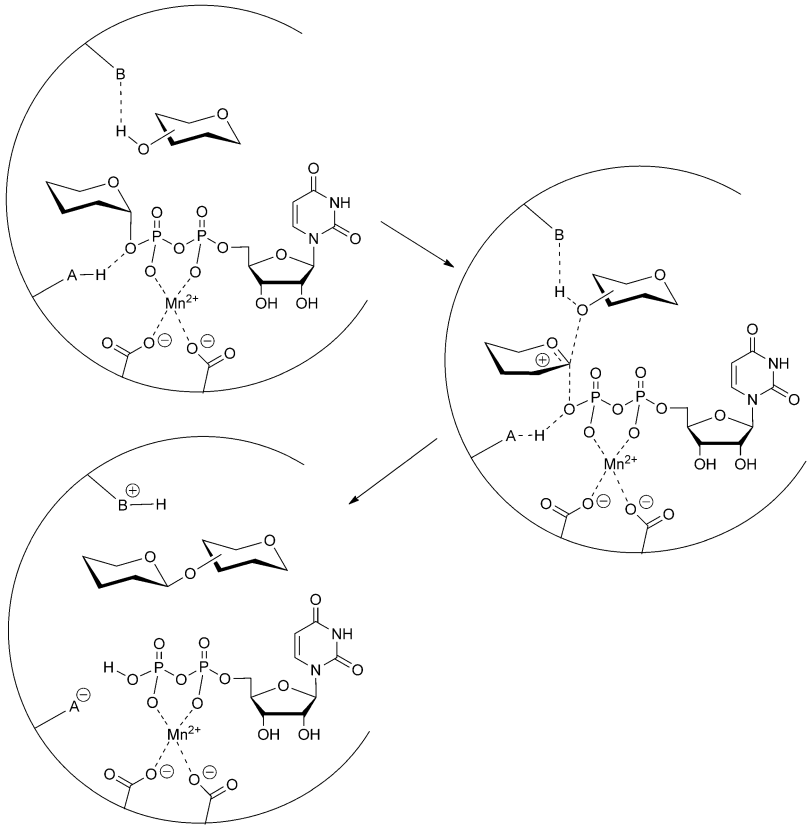

Figure 1. Proposed mechanism for an inverting metal-dependent glycosyltransferase.

these considerations, we have designed neutral donor analogues incorporating a pyridine scaffold connected to the carbohydrate moiety through a series of covalent bonds to functionalize the pyridyl moiety with a carbohydrate and a nucleoside (Figure 2).

The carbohydrates used are galactose as the natural moiety for galactosyltransferases and glucose as a negative control. The conjugation of the carbohydrate, pyridine, and nucleoside building blocks was achieved through a combination of glycosylation,[47] the Staudinger–Vilarrasa reaction,[48–50] and the Cu^{I}-catalyzed azide–alkyne cycloaddition.[51–53] The chemical functionalities connecting the three units were selected for their convenient synthesis and for their ability to interact with the Mn^{2+} ion in the active site of the respective enzyme. The natural α stereochemistry at the anomeric center of the carbohydrate does not necessarily need to be identical to the natural NDP sugar because β anomers have also been identified as GT inhibitors.[37] The neutral inhibitors were then evaluated as inhibitors with a panel of five recombinant galactosyltransferases (GalTs). These enzymes include the inverting enzyme bovine β-1,4-GalT and four retaining enzymes: bovine α-1,3-GalT, human blood group B-synthesizing galactosyltransferase α-1,3-GalT (GTB), murine dual specificity blood group A/B-synthesizing α-1,3-GalT/GalNAcT (AAGlyB), and *Neisseria meningitides* α-1,4-GalT. The best inhibitors of AAGlyB were then selected for crystallographic studies to determine their mode of interaction with the enzyme.

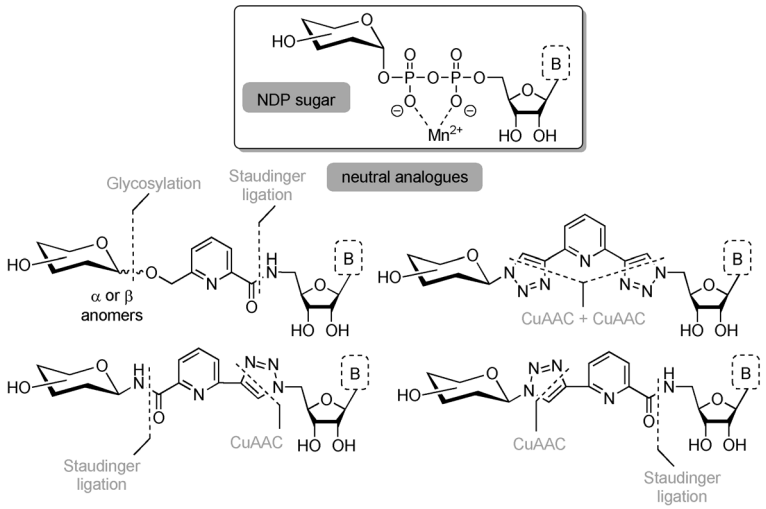

Figure 2. Structures of the neutral NDP-sugar analogues synthesized by a combination of glycosylation, the Staudinger–Vilarrasa reaction, and the copper-catalyzed azide–alkyne cycloaddition (CuAAC).

Results and Discussion

Synthesis of the inhibitors: The combination of glycosylation and the Staudinger–Vilarrasa reaction provided rapid access to the glucose- and galactose-based GT inhibitors **8** from the commercially available pyridine diester derivative **1** (Scheme 1, pathway A). After mono-reduction to alcohol **2**,[54] glycosylation of the 6-hydroxymethylpyridine derivative **2** provided the β-glycosides **4** in good yields after a careful investigation[47] of the glycosylation conditions required for this type of basic acceptor with

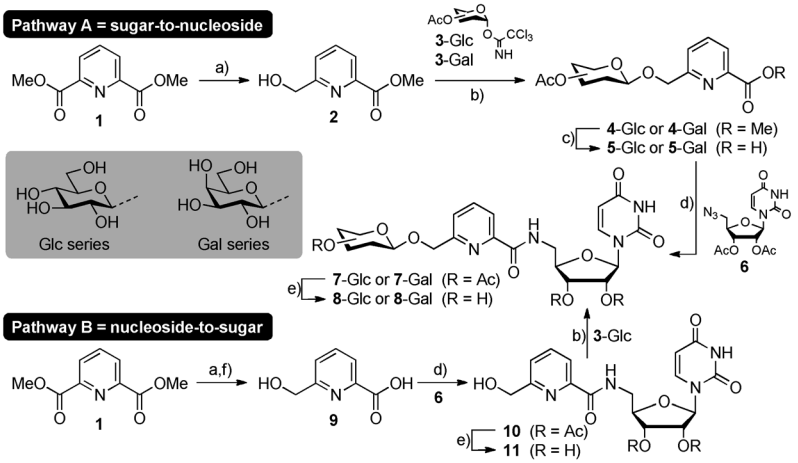

Scheme 1. Synthesis of the neutral GT inhibitors by using a combination of glycosylation and a Staudinger–Vilarrasa reaction by following two different pathways. Reagents and conditions: a) $NaBH_4$, $MeOH/CH_2Cl_2$, RT, 3 h, 56%. b) $BF_3{\cdot}Et_2O$, CH_2Cl_2, −20°C, 2 h, 53% **4**-Glc, 46% **4**-Gal, 33% **3**-Glc. c) NaI, C_5H_5N, 120°C, 5 h, 52% **5**-Glc, 76% **5**-Gal. d) PMe_3, diisopropylcarbodiimde (DIC), 1-hydroxybenzotriazole (HOBt), THF, RT, 16 h, 61% **7**-Glc, 31% **7**-Gal, 17% **10**. e) NaOMe, MeOH, 63% **8**-Glc, quantitative **8**-Gal and **11**. f) NaOH, $MeOH/H_2O$, 100°C (μW), 10 min, quantitative. Ac = acyl.

trichloroacetimidate glycosyl donors.[55–57] The methyl ester was then converted to the acid giving compounds **5**, which were used in a Staudinger–Vilarrasa reaction with the azido-uridine **6**[58] to afford the acetylated amides **7**. Final removal of the ester protecting groups gave the desired GT inhibitor candidates **8**. Similarly, the analogous synthesis was performed by first introducing the nucleoside and then the carbohydrate to obtain a more flexible synthetic approach (Scheme 1, pathway B). The mono-ester **2** was converted to the acid **9**, which was conjugated with the azido-uridine **6** to afford the amide **10**, which underwent glycosylation to provide the glycosides **7**.

The "sugar-to-nucleoside" approach was similarly used to generate the α-galactose series (Scheme 2) to determine the influence of the anomeric configuration on the inhibition of the various GTs. For this purpose, the 6-hydroxymethylpyridine derivative **2** was glycosylated with the benzylated galactosyl donor **12** to provide the α-galactoside **13**. At this point, debenzylation under hydrogenolysis conditions (H_2 1–8 atm, Pd/C) did not affect the benzyl ethers but rather reduced

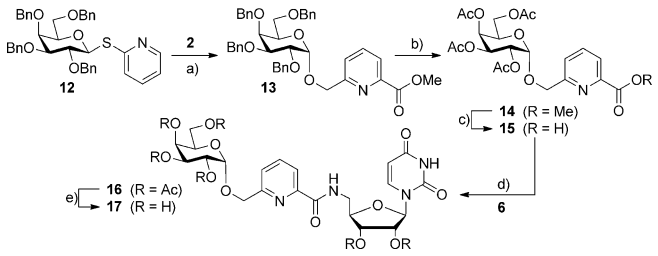

Scheme 2. Synthesis of the α-galactoside inhibitor candidate **17** through glycosylation and a Staudinger–Vilarrasa reaction. Reagents and conditions: a) MeI, CH_2Cl_2, 50°C, 78 h, 75%. b) i) $NaBrO_3$, $Na_2S_2O_4$, EtOAc/H_2O, RT, 2 h, then ii) Ac_2O, C_5H_5N, RT, 3 h, 42%. c) NaI, C_5H_5N, 120°C, 5 h, quantitative. d) PMe_3, DIC, HOBt, THF, RT, 16 h, 27%. e) NaOMe, MeOH, 63%. Bn = benzyl.

the pyridine ring to a piperidine as a mixture of diastereoisomers as observed by ^1H NMR spectroscopy and mass spectrometry ($m/z = 696.2$ for $[M+H]^+$). The benzyl ethers were therefore removed under oxidative conditions[59,60] and the crude mixture was then re-acetylated to provide the acetyl-protected compound **14**. The next synthetic steps were identical to those presented earlier with transformation to acid **15**, formation of the amide bond in compound **16**, and final removal of the acetate protecting groups to obtain the desired GT inhibitor candidate **17**.

The influence of the pyridine ring upon binding to the active site of the enzyme can also be evaluated by the synthesis of a benzene-based inhibitor candidate **21** in which the pyridine ring is replaced by a benzene moiety (Scheme 3). The

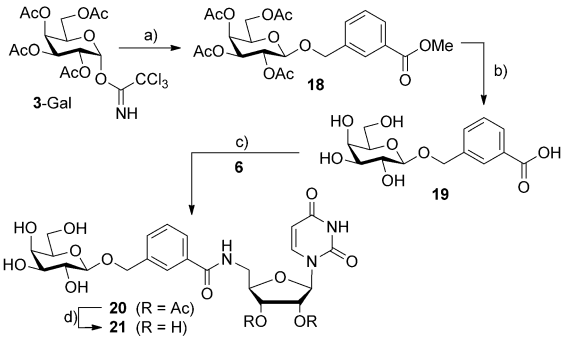

Scheme 3. Synthesis of a benzene-based pyrophosphate analogue through β-galactosylation and a Staudinger–Vilarrasa reaction. Reagents and conditions: a) methyl 5-hydroxymethylbenzoate, $BF_3{\cdot}Et_2O$, CH_2Cl_2, −20°C, 1 h, 79%. b) LiOH, THF/H_2O, RT, 48 h, 93%. c) PMe_3, DIC, HOBt, THF, RT, 16 h, 43%. d) NaOMe, MeOH, 73%.

trichloroacetimidate galactosyl donor **3**-Gal was used to obtain the galactoside **18** and the next steps were performed under the "sugar-to-nucleoside" strategy. The only difference here was the complete hydrolysis of the ester and methyl ester protecting groups to afford the hydroxylated acid **19**, because the sodium iodide/pyridine method provided poor results. The Staudinger–Vilarrasa reaction with the azido-uridine **6** afforded the partially acetylated amide **20**, which was converted to the hydroxylated GT inhibitor candidate **21**.

Four neutral NDP-sugar analogues were synthesized around a central pyridine scaffold, bearing a carbohydrate

moiety on one hand and an uridine on the other (Scheme 4). The carbohydrate and uridine moieties were conjugated to the pyridine through an amide and triazole linker, respectively or vice versa. Compounds were prepared

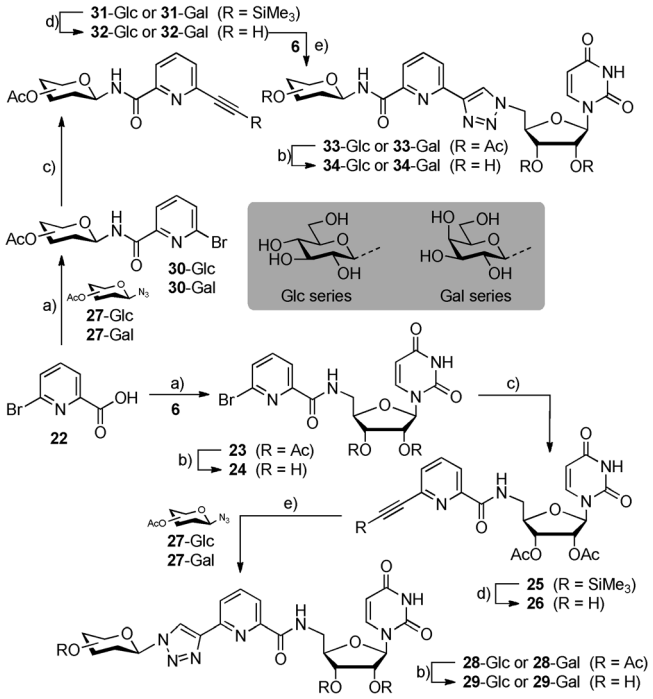

Scheme 4. Synthesis of two different series of neutral GT inhibitors by using a combination of the Staudinger-Vilarrasa reaction and CuAAC. Reagents and conditions: a) PMe_3, DIC, HOBt, THF, RT, 16 h, 37% **23**, 78% **30**-Glc, quantitative **30**-Gal. b) NaOMe, MeOH, 28% **24**, 78% **29**-Glc, 80% **29**-Gal, 85% **34**-Glc, 78% **34**-Gal. c) $Me_3SiC{\equiv}CH$, $[Pd(PPh_3)_4]$, CuI, iPr_2NH, PhMe, RT, 90% **31**-Glc, 93% **31**-Gal. d) nBu_4NF, THF/MeOH, RT, 4 h, 50% for two steps to **26**, 77% **32**-Glc, 79% **32**-Gal. e) $CuSO_4$, sodium ascorbate, tBuOH/H_2O, 35 °C, 68 h, 80% **28**-Glc, 44% **28**-Gal, 83% **33**-Glc, 64% **33**-Gal.

in the glucose and galactose series. Both syntheses started from the commercially available 6-bromopicolinic acid **22**, which was conjugated to the azido-uridine **6** under Staudinger–Vilarrasa reaction conditions to afford amide **23**. This intermediate could be deprotected to provide the uridine diphosphate (UDP) analogue **24** used in the enzymatic assays. Meanwhile, a Sonogashira reaction between the bromo-pyridine derivative **23** and trimethylsilylacetylene afforded the alkynylated pyridine derivative **25**, which was readily converted to the terminal alkyne **26**. A mixture of alkynylsilane (e.g., **25**) and terminal alkyne (e.g., **26**) was always obtained from the Sonogashira coupling reactions. This mixture can be readily converted into the desired terminal alkyne by using fluoride ions. The formation of this mixture of silyl-protected and terminal alkynes can be rationalized from the sila-Sonogashira–Hagihara coupling reactions reported by Nishihara and co-workers from alkynylsilanes.[61–66] In our case, trimethylsilylacetylene reacted under standard Sonogashira reaction conditions or through the silyl end under sila-Sonogashira–Hagihara conditions to provide either the trimethylsilyl (TMS)-protected or the terminal alkyne, respectively. Conjugation of the terminal alkyne **26** with the glycosyl azides **27** under CuAAC conditions provided the NDP-sugar analogues **28**, which were deprotected to the GT inhibitor candidates **29**. To reverse the positions of the amide and the triazole moieties, a similar synthesis was carried out from acid **22** with the formation of the amide bond with the glycosyl azides **27** to obtain the amides **30**. Subsequent Sonogashira coupling, deprotection of the silyl group, CuAAC conjugation with the azido-uridine **6**, and solvolysis of the acetate protecting groups afforded the desired GT inhibitor candidates **34**. The conditions used here for the CuAAC conjugations are the conditions reported by Sharpless and co-workers,[52] which uses Cu^{II} reduced in situ to Cu^{I} with sodium ascorbate. The present synthesis is the only case in which we have obtained better results under these conditions compared to the conditions used by Meldal and co-worker,[53] that is, using CuI as the source of Cu^{I}.

The last series of GT inhibitors involved the conjugation of the building blocks with two triazole groups obtained from the corresponding bis-alkynylated pyridine moiety and the azido-functionalized carbohydrates and nucleoside. We initially carried out sequential reactions for the glucose series (Scheme 5). However, a "one-pot" reaction not only expedited the synthesis but also led to better overall yields for the galactose compound **42** (Scheme 6).

The 2,6-dibromopyridine **35** was selectively mono-alkynylated under Sonogashira reaction conditions to the silylated

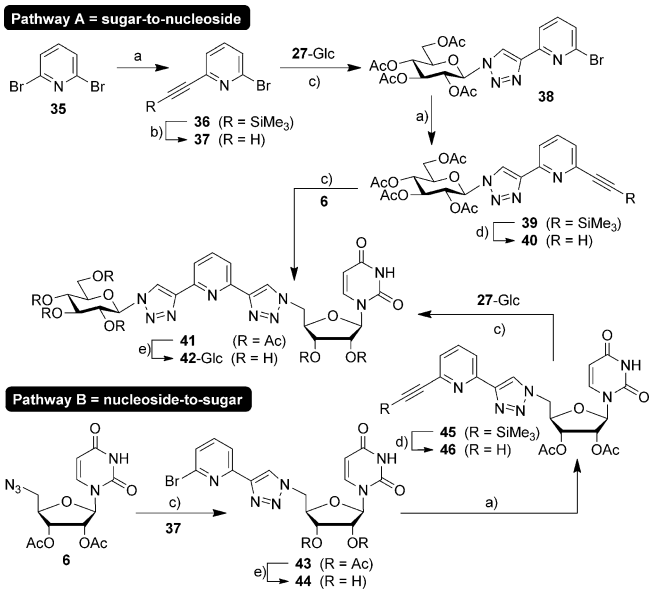

Scheme 5. Synthesis of a 2,6-bis-triazolyl-pyridyl-based neutral GT inhibitors by using two subsequent CuAAC conjugations. Reagents and conditions: a) $Me_3SiC{\equiv}CH$, $[Pd(PPh_3)_4]$, CuI, iPr_2NH, PhMe, RT, 71% **45**, 95% **39**. b) K_2CO_3, THF/MeOH, RT, 2 h, 79% for two steps to **37**. c) CuI, iPr_2NEt, DMF, 100 °C (μW), 15 min., 93% **38**, 74% from **40** to **41** and 86% from **46** to **41**, 95% **43**. d) nBu_4NF, MeOH, RT, 4 h, 96% **40**, 52% **46**. e) Et_3N, MeOH, H_2O, RT, 82% from **41** to **42**-Glc or NaOMe, MeOH, 39% from **41** to **42**-Glc and 82% from **43** to **44**.

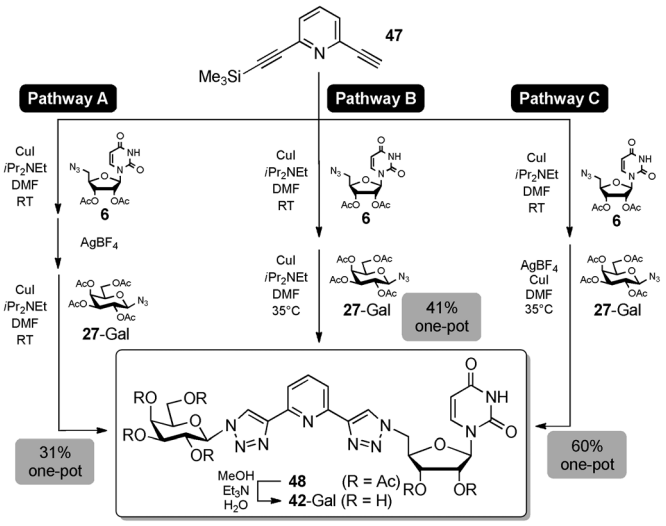

Scheme 6. "One-pot" synthesis of a 2,6-bis-triazolyl-pyridyl-based neutral GalT inhibitor by using sequential CuAAC cycloadditions.

intermediate **36**, which was converted to the terminal alkyne **37** (Scheme 5, pathway A). CuAAC conjugation with the glucosyl azide **27**-Glc afforded the bromo-intermediate **38**, which underwent another Sonogashira coupling to obtain compound **39**, which was converted to the desired terminal alkyne **40**. Final CuAAC cycloaddition with the azido-uridine **6** and removal of the ester protecting groups gave the desired GT inhibitor candidate **42**-Glc. The synthesis was performed similarly from the nucleoside to the sugar moiety (Scheme 5, pathway B). The azido-uridine **6** was conjugated with the terminal alkyne intermediate **37** to afford the triazole derivative **43**. This compound was converted to its hydroxylated counterpart **44** as an analogue of UDP for evaluation in enzymatic assays. The rest of the synthesis was identical to the preceding reactions to obtain **42**-Glc.

The introduction of several orthogonally protected alkyne moieties on a multivalent scaffold provides a rapid access to hetero-functionalized compounds through CuAAC conjugations with sequential deprotection of the alkyne groups.[67–69] In this context, we used the desymmetrized 2,6-bis-acetylene pyridine derivative **47**[69] as the central scaffold for the synthesis of our target GT inhibitor candidate. This synthesis was performed for the galactose series (Scheme 6). Our initial attempt was performed under the conditions described by Aucagne and Leigh[68] in which an initial CuAAC coupling with the azido-uridine **6** was followed by a selective removal of the silyl protecting group with silver tetrafluoroborate to allow a second CuAAC coupling with the galactosyl azide **27**-Gal (Scheme 6, pathway A). Although the overall yield reported by Aucagne and Leigh[68] was almost quantitative (>95%) by using other azide and alkyne derivatives, we could not isolate the desired acetylated derivative **48** in more than 31% yield. When further investigating the reaction conditions, we observed that a slight increase in temperature was sufficient to remove the silyl protecting group (Scheme 6, pathway B). The overall yield increased to 41% (Scheme 6, pathway B) and only two additions of reagents were required because silver salts were not used. We obtained a yield of 60% when silver salts were introduced with the second addition of the galactosyl azide **27**-Gal (Scheme 6, pathway C). This sequential double-CuAAC synthetic strategy involves three synthetic steps performed with two subsequent additions of reagents in a "one-pot" procedure leading to a global yield of 60%, which corresponds to 84% yield for each reaction step. The desired acetylated compound **48** could therefore be obtained in a minimum number of steps and from readily available starting materials. The acetate protecting groups were then removed to afford the target GT inhibitor candidate **42**-Gal.

The syntheses of ten GT inhibitor candidates were therefore achieved in a minimum number of steps from readily available starting materials by using several conjugation techniques between the carbohydrate, the pyridine scaffold, and the nucleoside such as glycosylation, the Staudinger–Vilarrasa reaction, and "click" chemistry (CuAAC). The ten molecules (Figure 3) are classified as GalT inhibitor candidates for the galactose-containing derivatives **8**-Gal, **17**, **21**, **29**-Gal, **34**-Gal, and **42**-Gal, whereas the glucose-based compounds **8**-Glc, **29**-Glc, **34**-Glc, and **42**-Glc were synthesized as negative controls or for the assessment of the influence of the carbohydrate on the selectivity or inhibitory properties towards the enzymes. The two UDP analogues **24** and **44** were also prepared to obtain data about the influence of the carbohydrate on the inhibition and also as model compounds because UDP is a known inhibitor of UDP-sugar-utilizing GTs.

Inhibition studies: All twelve compounds were first evaluated as inhibitors of five galactosyltransferases at a concentration of 1 mM of inhibitor by using K_m concentrations of the donor and high concentrations of the acceptor substrates (Table 1). Compound **8**-Gal was the best inhibitor in the series with 80–100% inhibition of the five enzymes. This analogue has the opposite β-anomeric configuration as the natural UDP-Gal donor. Interestingly, the α-anomer **17** also inhibited the enzymes, though it was somewhat weaker with 37–97% inhibition. Compound **8**-Glc was a very weak inhibitor of all enzymes except for AAGlyB, where 47% inhibition was observed. The nature of the glycoside is important for the inhibition of the enzymes. However, the most active compound **8**-Gal inhibited all of the enzymes, thus selectivity will require further modifications in the design of the neutral GT inhibitors.

The bromo-pyridine analogue of UDP, namely compound **24**, which lacks a monosaccharide, was a weaker inhibitor. The introduction of a carbohydrate moiety enhances the inhibition of the GTs. Compound **21** with benzene rather than pyridine was less effective for the retaining enzymes with 19–39% inhibition, whereas the inverting β-1,4-GalT was inhibited by 78%. Therefore, the influence of the nitrogen atom in the pyridine-containing inhibitors is crucial but not critical as explained later in the crystallographic studies.

Compound **42**-Glc with the bis-triazolyl pyridine was a potent inhibitor of β-1,4-GalT (100% inhibition) and a

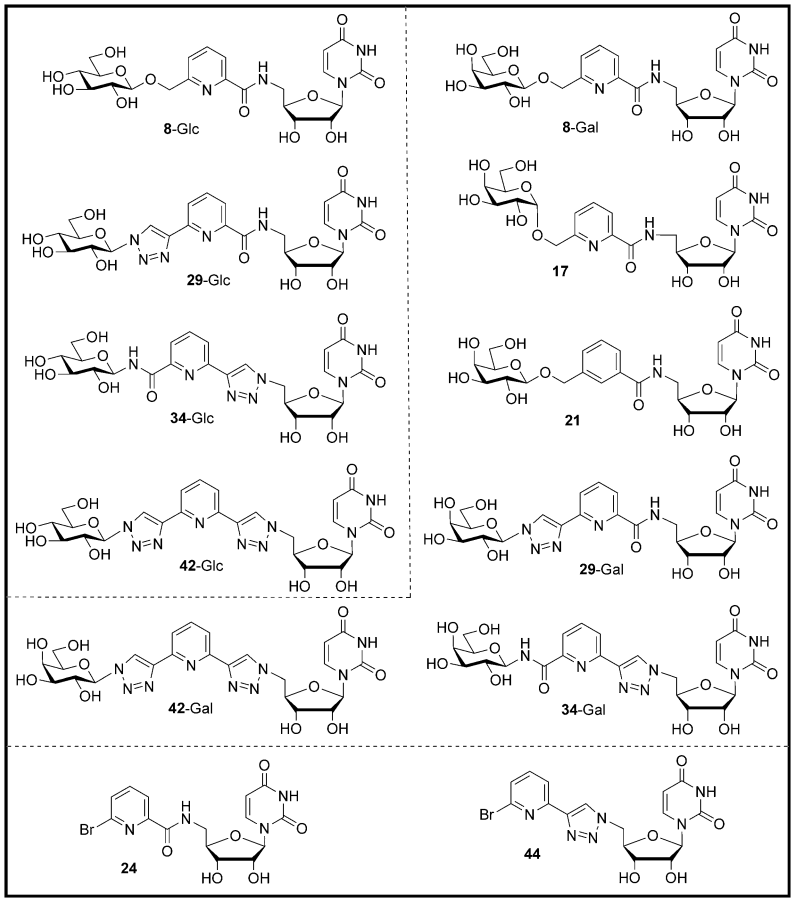

Figure 3. Structures of the twelve GT inhibitors synthesized within this study.

weak inhibitor of the retaining enzymes (30–36% inhibition). Surprisingly, **42**-Gal was a weaker inhibitor than **42**-Glc. Compounds **29** and **34**, which contain the triazolyl pyridine moiety, were also weak inhibitors. In these series, the influence of the carbohydrate moiety was less significant than for compounds **8**.

The most active compound **8**-Gal was next evaluated as a competitive inhibitor of UDP-Gal by using high concentrations of the acceptor and varying the concentration of the inhibitor at low and high concentrations of the donor. Non-linear curves were seen in Dixon plots for AAGlyB and β-1,4-GalT, suggesting a complex mode of inhibition (Figure 4as well as Figures S1 and S5A in the Supporting Information). This complex behavior was confirmed in Michaelis–Menten plots, which showed mixed inhibition with effects on both V_{max} and K_m at high concentrations of **8**-Gal (Figure 5 as well as Figures S2 and S6 in the Supporting Information).

Compound **8**-Gal was also a mixed inhibitor of α-1,4-GalT (Figure S8 in the Supporting Information), α-1,3-GalT (Figure S10 in the Supporting Information), and GTB (Figure S12 in the Supporting Information, mixed at high inhibitor concentrations, competitive at low inhibitor concentrations). Non-linear Dixon plots were also obtained from evaluation of compound **17** with β-1,4-GalT (Figure S3 in the Supporting Information) and AAGlyB (Figure S5B in the Supporting Information). Michaelis–Menten plots confirmed that compound **17** was a mixed inhibitor of β-1,4-GalT at high concentrations (Fig-

Table 1. Kinetic enzymatic measurements of the inhibition of the GT inhibitors with five different GalTs.

Entry	Inhibitor	β-1,4-GalT		α-1,4-GalT		α-1,3-GalT		GTB		AAGlyB	
		inhibition[a] at 1 mM [%]	IC_{50}[b] (μM)	inhibition[a] at 1 mM [%]	IC_{50}[b] (μM)	inhibition[a] at 1 mM [%]	IC_{50}[b] (μM)	inhibition[a] at 1 mM [%]	IC_{50}[b] (μM)	inhibition[a] at 1 mM [%]	IC_{50}[b] (μM)
1	**8**-Glc	13		23		19		11		47	1220
2	**8**-Gal	100	152	80	546	99	320	84	262	93	493
3	**17**	97	334	37	1597	79	602	53	725	80	584
4	**21**	78	573	27		39	1020	23		19	
5	**29**-Glc	12		0		11		1		14	
6	**29**-Gal	34		2		11		10		22	
7	**34**-Glc	15		17		6		18		14	
8	**34**-Gal	0		8		26		38	2304	31	
9	**42**-Glc	100	634	33	1962	30	1061	36	1767	36	1417
10	**42**-Gal	15		11		22		34		19	
11	**24**	9		21		32		38	1231	40	1035
12	**44**	9		1		0		28		20	
13	uridine		>1000		>3000		>1000		1587		>1000
14	UMP[c]		313		>1000		130		10		2
15	UDP		25		62		53		5		1

[a] Compounds were evaluated at K_m concentrations of the donor and high concentrations of the acceptor substrate. [b] IC_{50} values were determined for selected inhibitors with 35–100% inhibition at 1 mM. [c] UMP = uridine monophosphate.

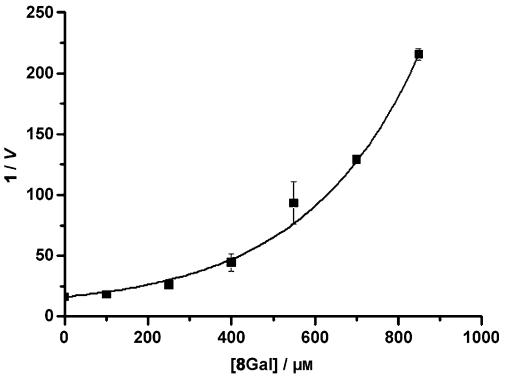

Figure 4. Non-linear Dixon plot of **8**-Gal inhibition of AAGlyB carried out at a saturating acceptor concentrations. The concentration of UDP-Gal was 0.7 μM, approximately the K_m for the donor, the concentration of the α-L-Fuc*p*-(1→2)-β-D-Gal*p*-OC_8H_{17} acceptor was 20 μM with six concentrations of **8**-Gal from 100–850 μM tested. Assays were carried out in duplicate showing non-linear dependence on the inhibitor concentration ($r^2 = 0.8684$ was obtained from linear regression analysis of the data points).

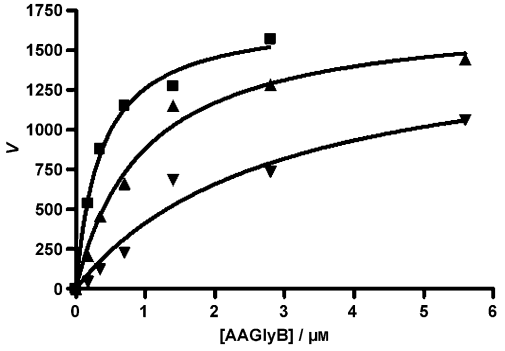

Figure 5. Michaelis–Menten plot of **8**-Gal inhibition of AAGlyB. The kinetics assays were carried out at concentrations of the donor of 0, 0.175, 0.35, 0.7, 1.4, 2.8, and 5.6 μM, the concentration of the acceptor α-L-Fuc*p*-(1→2)-β-D-Gal*p*-OC_8H_{17} was 20 μM with two concentrations of **8**-Gal (300 (▲) and 500 μM (▼), ■ = no inhibition). Non-linear regression analysis with GraphPad Prism[70] was used to obtain K_m and V_{max} values along with standard errors.

ure S4 in the Supporting Information), competitive with UDP-Gal for AAGlyB (Figure S7 in the Supporting Information), α-1,4-GalT (Figure S9 in the Supporting Information), and a mixed inhibitor of α-1,3-GalT and GTB at high concentrations (Figures S11 and S13 in the Supporting Information).

To obtain a relative ranking of the compounds with such complex inhibition patterns, IC_{50} measurements were carried out with selected inhibitors. For all enzymes, compound **8**-Gal (Table 1, entry 2) was a more potent inhibitor than uridine, suggesting that there are additional binding interactions with the pyridine scaffold. It was also a better inhibitor of β-1,4-GalT and α-1,4-GalT than UMP. It was somewhat less effective than UMP for α-1,3-GalT and much weaker than UMP for GTB and AAGlyB. The latter three retaining enzymes are all members of the GT family 6. The corresponding α-anomer **17** (Table 1, entry 3) was also more effective than uridine, though it was weaker than UMP. Removal of the nitrogen atom from the pyridine ring provided the weaker inhibitor **21** in these series (Table 1, entry 4), whereas the introduction of triazole moieties was also detrimental (Table 1, entries 5–10). The presence of glucose residues resulted in weaker inhibitory properties in comparison to the galactosylated derivatives. The neutral UDP analogue **24** did not inhibit the enzymes more potently than **8**-Gal or compound **17**, whereas analogue **44** was a weak inhibitor of the blood group enzymes and showed no inhibition of the other enzymes (Table 1, entries 11 and 12).

Crystallographic studies: To better understand the basis for the complex inhibition patterns and the preference for an analogue, which has the opposite anomeric configuration than the natural donor, the well characterized AAGlyB enzyme, which readily crystallizes was used to investigate the mode of binding of **8**-Gal, **17**, and **8**-Glc. Crystals of the apoprotein were soaked with the compounds and their structures solved and refined.

The protein structures in all three crystals are essentially identical and closely resemble that in PDB ID:2RJ7 for the AAGlyB mutant,[13] which includes an UDP-Gal molecule in the binding site. The root-mean-square deviation (RMSD) values after superposition show deviations of the α-carbon atoms of only 0.28 Å for **8**-Gal, 0.30 Å for compound **17** and 0.30 Å for **8**-Glc relative to PDB ID:2RJ7 (calculated with the SSM algorithm in Coot[78]). Our models extend to Ala58 in the N terminus and to Lys346 at the C terminus, the rest of the C-terminal tails is disordered and invisible in the electron density maps. Residues 58–63 are from the cloning vector with the AAGlyB sequence starting at Val64.

All three inhibitors are bound to the protein in a nearly identical manner. The uracil and the ribose group overlap very closely with those in PDB ID:2RJ7, with the linker to the pyridine ring also in a conformation resembling that of the first phosphate group in UDP-Gal (Figure 7). The interactions of the uracil and the ribose group with the protein are all conserved. The conformation of the pyridine ring deviates strongly from that of the phosphates in UDP-Gal, with the ring extending roughly perpendicularly to and away from the uracil. The amide group and the anomeric oxygen atoms, together with the pyridine nitrogen atom, chelate the Mn^{2+} ion, which is displaced from its position in GTA/GTB as will be described below. The hydroxyl oxygen atom of Tyr126, which has a stacking interaction with the uracil, it is in van der Waals contact with the pyridine ring of the inhibitors, with its hydroxyl group roughly in the center of the π cloud of the pyridine. For **8**-Gal, we observed two alternative positions of the anomeric oxygen atom of the galactose, only one of which is coordinated to manganese. The galactose group itself was not visible in the electron density and has not been modeled. It is likely disordered between many different conformations. In the case of compound **17**, two alternative conformations of the anomeric oxygen atom were

also observed. In the one coordinating to manganese, the galactose is again not visible and was not modeled, whereas in the alternative conformation weak electron density was visible for the galactose group, which was modeled with reduced occupancy (Figure 6). The oxygen atom O5′ of this

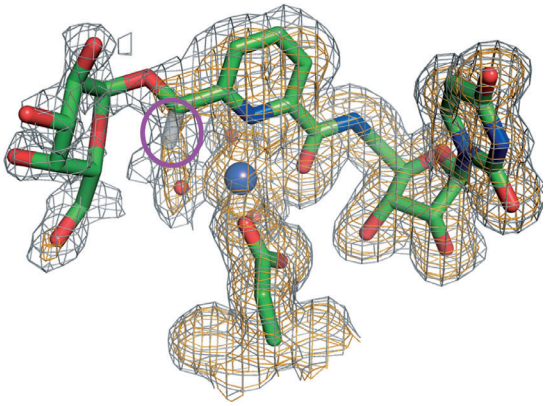

Figure 6. Electron density for the inhibitor, manganese, and its ligands in the structure of compound **17** (PDB ID:4KC4). The anomeric oxygen atom is observed in two alternative conformations, but the galactose could only be modeled for one of them. The second conformation, with only the oxygen atom visible as a transparent rod, is marked with the pink circle. The orange mesh is electron density from the $2F_o-F_c$ map contoured at 1.0σ, whereas the gray mesh is the same map contoured at 0.4σ. The side chain in the lower part is from Asp213.

galactose comes into close contact with the oxygen atom O3 of the fucose moiety of the acceptor in an area where the electron density difference map suggests disorder. Additional conformations are probably available for the group in this area. The final B-factors for this galactose, which was modeled at half occupancy, are similar to those of the rest of the inhibitor molecule, modeled with full occupancy. We did not attempt to refine the occupancy of the galactose, but this suggests it to be close to 50% in the modeled conformation. For **8**-Glc, only the chelating conformation of the anomeric oxygen atom was observed, whereas the glucose was invisible in the electron density, it is either disordered or hydrolyzed. The presence of the galactose in compound **17** hints at all hexoses being present in the crystals, only in disordered conformations. In any case, the pyridine ring projects the hexopyranoses to a different position to what they occupy in the tucked-under conformation observed for PDB ID:2RJ7 (Figure 7) and away from the galactose of the acceptor. The pyridine ring in the inhibitors is roughly occupying the same space as the side chains of Lys346, Arg352, and, to a lesser extent, His348 would in the closed conformation[13] in which the basic side chains of Lys346 and Arg352 coordinate the pyrophosphate and stabilize it as a leaving group. Hence, it is likely that the inhibitors are responsible for the disorder of the C-terminal tails in all three structures.

The manganese cation is affected by the chelating inhibitors and displaced from the position it normally occupies. In the structures of GTA and GTB, a Mn^{2+} ion is bound to the carboxylic groups of Asp211 and Asp213, as well as to the pyrophosphate of UDP or UDP-Gal. In our structures, that position is occupied by a water molecule, which is in the coordination sphere of the manganese ion and hydrogen bonded to the amide carbonyl atom of the inhibitors, to Asp211 and to Asp213. The manganese ion itself is displaced by more than 2 Å, away from Asp211, and is therefore not bound to this residue but only to Asp213, and that through the other carboxylic oxygen atom. Both side chains of Asp211 and Asp213 are slightly displaced as a result (Figure 7).

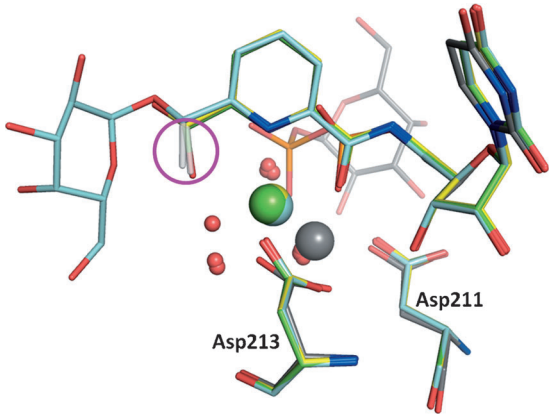

Figure 7. Superposition of all three inhibitors and UDP-Gal from PDB ID:2RJ7. PDB ID:2RJ7 is shown with gray carbon atoms, **8**-Gal with yellow carbon atoms, compound **17** with cyan carbon atoms, and **8**-Glc with green carbon atoms. Compounds **8**-Gal and **17** adopted a second conformation for the anomeric oxygen atom colored transparent white and shown inside the pink circle; the sugars, likely disordered, are not visible in the electron density for those conformations. For UDP-Gal, the phosphates and the galactose can be seen in the back in orange and gray. Also included as sticks are Asp211 and Asp213 with the same color code. The large spheres are the manganese cations, colored as the corresponding carbon atoms. Also shown as smaller red spheres are the water molecules in the coordination spheres of all three inhibitors.

The environment of the manganese ion will be described for **8**-Glc because the other two structures are very similar with slightly longer distances to the anomeric oxygen atom, which can be a result of the different occupancies or of geometric compromises during refinement due to the modeling of the disorder for that atom but not for the rest of the inhibitor (Figure 8). The Mn^{2+} ion is hepta-coordinated with ligand distances mostly longer than those in the tetra-coordinated structures with UDP or UDP-Gal. The coordination sphere can be described as a pentagonal bipyramid with three of the equatorial positions occupied by the pyridine nitrogen atom and its adjacent carboxylic oxygen atoms at 2.3, 2.5, and 2.3 Å, respectively (Figure 8). These three atoms, the pyridine ring, and the manganese ion are coplanar. The last two equatorial positions in the coordination sphere of the manganese ion are occupied by bound water molecules at 2.3 and 2.4 Å, respectively. The latter is markedly anisotropic, sitting in elongated electron density (it is only half occupied in the other two structures), likely as a

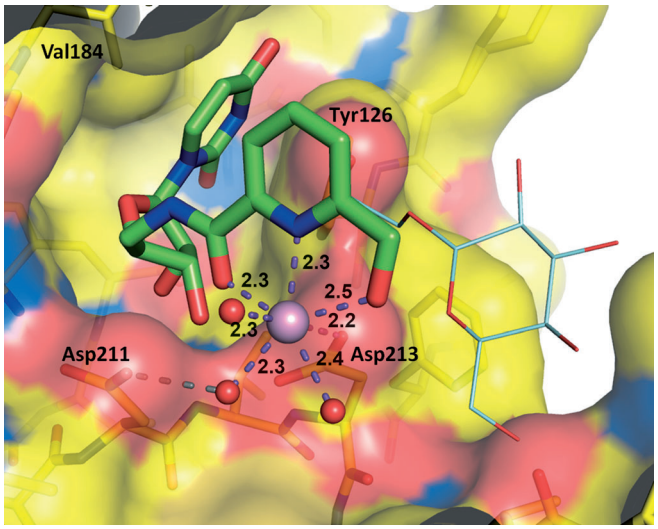

Figure 8. Coordination spheres of the manganese ion in the **8**-Glc complex (PDB ID:4KC1) structure. **8**-Glc is shown in thick sticks with green carbon atoms, the alternative conformation for compound **17** is shown in thin sticks with blue carbon atoms, showing the galactose. The manganese ion is shown in pink. AAGlyB in the **8**-Glc crystal is shown as a semitransparent surface representation colored according to the closest atom and containing a stick model of the protein with yellow carbon atoms.

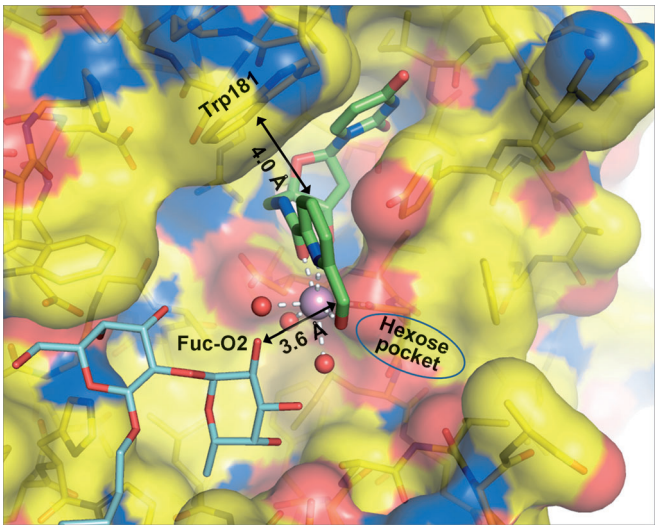

Figure 9. Overall mode of the binding of **8**-Glc. The protein is represented as a semitransparent surface with a stick model inside with yellow carbon atoms, **8**-Glc is represented as a thick stick model with green carbon atoms. The acceptor α-L-Fuc*p*-(1→2)-β-D-Gal*p*-OC_8H_{17} is represented with thin sticks and cyan carbon atoms. The manganese ion is the large purple sphere and the white dashed lines indicate its coordination ligands, which include three water molecules (small red spheres). Black arrows indicate the distances mentioned in the text.

result of spatial disorder arising from alternative conformations of the anomeric oxygen atom. The two axial positions are filled by a water molecule at 2.3 Å and a carboxylic oxygen atom from Asp213 at 2.2 Å.

In all three crystals the internal loop adopts a structure similar to that in PDB ID:2RJ7,[13] which is in the fully closed conformation. In our structures a continuous chain could be modeled throughout this area but with evident signs of disorder for the amino acids 194–198. Arg176, the first of the four mutations in AAGlyB, has a disordered side chain and has only been modeled to the β-carbon atom. The acceptor α-L-Fuc*p*-(1→2)-β-D-Gal*p*-OC_8H_{17} adopts the same position, conformation, and interactions with the protein as in PDB ID:2RJ7, but in our structures its aliphatic chain has been modeled fully to the eighth carbon atom (Figure 9). Taken together, the multiple effects of the inhibitors on metal chelation and displacement along with potential interference with the folding of the protein loops will result in the complex kinetic inhibitory patterns that were observed.

The mode of binding of these inhibitors prevents the folding of the C-terminal tail of AAGlyB, creating opportunities for the further modification of the inhibitors to increase their affinities or their specificities. The uracil and the ribose are bound in a crevice at the surface of the protein in the same way as UDP-Gal, but the pyridine ring extends into what, in the absence of an ordered C-terminal tail, is now the surface of the protein (Figure 9). An aliphatic group substituted in 4-position of the pyridine would be ideally placed, 4 Å away and at a favorable angle, to create stacking or van der Waals interactions with the side chain of Trp181, whereas the 5-position of the pyridine creates the opportunity for other interactions mediated by longer linkers. The glucose and the galactose substituents in the inhibitors described here are mostly not visible in our electron density, most likely disordered into what is shown as the "hexose pocket" in Figure 9. They could be modified to make a more defined interaction. Their glycosidic oxygen atom is in the proximity of the fucose residue from the acceptor. In particular, the carbon atom between the pyridine and the hexoses is only 3.6 Å away from the oxygen atom O2 of the fucose (Figure 9). Hence, a substituent in that carbon atom could easily occupy the space where the acceptor binds. A very short, flexible group could then act as a covalent linker to a fucose or a Fuc-Gal substituent, in the case of AAGlyB, or to a different acceptor or acceptor analogue for other glycosyltransferases, thus creating a bisubstrate inhibitor.[18] This should result in an increase in both the affinity and the specificity of the inhibitors.

Conclusion

The design of glycosyltransferase inhibitors is an active and growing field of research at the interface of organic synthesis, carbohydrate chemistry, and biology. The design of GT inhibitors requires the careful analysis of the structural features of the substrates (NDP sugars) and the acceptors of the enzymes to which the carbohydrate residue is transferred. The importance of a cation in the active site of metal-dependent GTs prompted the design of several NDP-sugar analogues with variations at the carbohydrate or nucleoside

moieties, but also frequently to the pyrophosphate moiety. Nevertheless, neutral inhibitors are now being investigated to provide cell-permeable substrates for potential cellular studies or in vivo applications as fundamental tools for biology or as potential drugs. The design and synthesis of ten GT inhibitors was performed from a desymmetrized pyridine motif by using a combination of conjugations through *O*-glycoside, amide bond, or triazole functionalities. Their inhibition towards five enzymes provided useful structure–activity relationships for such GTs. The inhibitions observed were always weaker than for UDP and this could represent a limitation for applications in cellular assays. More interestingly, co-crystals of three inhibitors in the active site of AAGlyB could be obtained, which showed the chelation of the manganese ion with the pyridine portion of the designed neutral GT inhibitors. The carbohydrate moieties of these three co-crystallized inhibitors did not occupy the expected position as in the natural UDP-Gal substrate. Rather the carbohydrate occupied the "hexose pocket" and pointed into the solvent. Limited contacts with the enzyme also explain the poor selectivity observed with respect to the hexose (galactose or glucose) present in the inhibitor.

Experimental Section

Materials and general methods: All reagents were obtained from commercial sources and used without further purification. Dichloromethane and acetonitrile were distilled over CaH_2. Methanol was distilled over Mg/I_2. All reactions were performed under an argon atmosphere unless otherwise stated. Thin-layer chromatography (TLC) was carried out on aluminum sheets coated with silica gel 60 F_{254} (Merck). TLC plates were inspected by UV light ($\lambda = 254$ nm) and developed by treatment with a mixture of 10% H_2SO_4 in EtOH/H_2O (1:1 v/v) followed by heating. Silica gel column chromatography was performed with silica gel Si 60 (40–63 μm). NMR spectra were recorded at 293 K, unless otherwise stated, by using Bruker 300, 400, or 500 MHz spectrometers. Chemical shifts are referenced relative to deuterated solvent residual peaks. The following abbreviations are used to explain the observed multiplicities: s = singlet, d = doublet, t = triplet, q = quadruplet, m = multiplet, and br = broad singlet. Complete signal assignments were based on 1D and 2D NMR (COSY, HSQC, and HMBC correlations). High-resolution (HR-ESI-QToF) mass spectra were recorded by using a Bruker MicroToF-Q II XL spectrometer. Optical rotations were measured by using a Perkin–Elmer polarimeter and values are given in $10^{-1}{}^\circ\,cm^2\,g^{-1}$. AAGlyB was cloned and expressed in *Escherichia coli* (*E. coli*) by using standard mutagenesis techniques.[71,72] All other GalTs were expressed and purified as previously described,[35,73,74] apart from β-1,4-GalT, which was obtained commercially from Sigma–Aldrich.

General protocol for the Staudinger–Vilarrasa conjugation: The acid (0.466 mmol, 1 equiv) and HOBt (0.839 mmol, 1.8 equiv) were co-evaporated with toluene (3×5 mL) and THF (3×5 mL). The mixture was dried under vacuum for 1 h. The mixture was dissolved in dry THF (4 mL) under argon and cooled to 0 °C. DIC (0.839 mmol, 1.8 equiv) was added dropwise at 0 °C. After addition, the ice bath was removed and the reaction was stirred at RT for 30 min. Meanwhile, the azide (0.699 mmol, 1.5 equiv) was dissolved in dry THF (4 mL) under argon and cooled to 0 °C. PMe_3 (0.932 mmol, 2 equiv) was added and the reaction was stirred at 0 °C. After 30 min, the solution was transferred into the flask containing the acid/HOBt solution at 0 °C. The flask was washed with THF (4 mL) and the solution was transferred. The resulting reaction mixture was stirred at 0 °C for 1 h then allowed to reach RT and stirred for additional 16 h. The reaction mixture was diluted with water (60 mL) and extracted with EtOAc (4×60 mL). The combined organic layers were washed with a saturated aqueous solution of Na_2CO_3 (60 mL), H_2O (60 mL), and brine (60 mL), dried (Na_2SO_4), and concentrated. The residue was purified by silica gel column chromatography (petroleum ether to EtOAc) to afford the desired amide.

General protocol for the Meldal CuAAC conjugation: $i Pr_2NEt$ (0.036 mmol, 0.25 equiv) was added into a flask containing the azide (0.14 mmol, 1 equiv), the alkyne (0.14 mmol, 1 equiv), and CuI (0.01 mmol, 0.1 equiv) in DMF (2 mL). The reaction was stirred at RT overnight. After 24 h, the solution was diluted with EtOAc (50 mL), washed with a saturated aqueous solution of Na_2CO_3 (2×25 mL) and H_2O (30 mL). The combined aqueous layers were extracted with EtOAc (3×30 mL). The combined organic layers were dried (Na_2SO_4) and concentrated. The residue was purified by silica gel column chromatography to afford the desired triazole.

General protocol for the Sharpless CuAAC conjugation: $CuSO_4$ (0.11 mmol, 0.6 equiv) and sodium ascorbate (0.228 mmol, 1.2 equiv) were added to a solution of the alkyne (0.19 mmol, 1 equiv) and the azide (0.19 mmol, 1 equiv) in *t*BuOH/H_2O (1:1, 5.6 mL:280 μL). The reaction mixture was stirred at 35 °C for 24 h, then diluted with water (20 mL), and extracted with CH_2Cl_2 (3×30 mL). The combined organic layers were dried (Na_2SO_4) and concentrated. The residue was purified by silica gel column chromatography to afford the desired triazole.

General protocol for the Sonogashira reaction: The bromo-arene (1.0 mmol, 1 equiv), $[Pd(PPh_3)_4]$ (0.1 mmol, 0.1 equiv), and CuI (0.1 mmol, 0.1 equiv) were dissolved in toluene (25 mL) and the solution was degassed with argon. Then, trimethylsilylacetylene (3.0 mmol, 3 equiv) and diisopropylamine (2.2 mmol, 2.2 equiv) were added. The reaction was stirred for 48 h at RT protected from light and then poured into a saturated aqueous solution of NH_4Cl (100 mL). The aqueous layer was extracted with CH_2Cl_2 (3×100 mL). The combined organic layers were washed with H_2O (100 mL) and brine (100 mL), dried (Na_2SO_4), and concentrated. The residue was then purified by silica gel column chromatography to afford the desired product.

Radiochemical inhibition assay: Radiochemical enzyme assays were performed in a final volume of 15 μL, containing the corresponding enzyme, radioactive-labeled UDP-[^{3}H]Gal, the requisite acceptor α-L-Fuc*p*-(1→2)-β-D-Gal*p*-OC_8H_{17}, β-D-GlcNAc*p*-O-$(CH_2)_8$-CO_2Me, or β-D-Lac*p*-O-$(CH_2)_8$-CO_2Me, and the inhibitor (0–3 mM). The reaction mixture was incubated in 3-morpholinopropanesulfonic acid (MOPS) buffer (50 mM), $MnCl_2$ (20 mM), pH 7.0, and bovine serum albumin (1 mg mL^{-1}) for a certain time at 37 °C (a time for which linear rates are obtained by using these assay conditions), and the reaction was quenched with cold water (400 μL). The enzymatic product was isolated by purification with Sep-Pak RC C-18 cartridges (Waters). Radioactivity was measured by using a Beckman Coulter LS 6500 multi-purpose scintillation counter.

Crystallization and structure refinement: Metal-free protein AAGlyB was crystallized at 20 °C by the sitting drop method with drops containing 1.6 μL of the protein stock and 1.6 μL of the reservoir solution containing 13 or 15% polyethylene glycol (PEG) 3350, 50 or 150 mM ammonium sulfate, and 50 mM MOPS, pH 7. Seeding was performed with a horse hair from previous similar drops, and the drops were allowed to equilibrate over 500 μL of the reservoir solution. Crystals of the apoform of the protein grew to a final size of approximately 200 μm in one week. Drop wells containing the best crystals were opened, 2.4 μL of 50 mM MOPS, pH 7, 50 mM $MnCl_2$, and 100 mM inhibitor were added followed by 0.8 μL of a 200 mM α-L-Fuc*p*-(1→2)-β-D-Gal*p*-OC_8H_{17} solution. The drops were mixed, resealed, allowed to equilibrate for 45 min, then opened again, and 3 μL of the reservoir solution mixed 1:1 with glycerol were added as cryoprotectant. After one minute, the crystals were mounted in Mitegen loops and flash frozen in liquid nitrogen. Diffraction data for crystals with the inhibitors **8**-Gal, **17**, and **8**-Glc were collected in Beamline ID23-2 at ESRF at a wavelength of $\lambda = 0.873$ Å with a crystal-to-detector distance of 167.5 mm with 1° oscillations, 180 images per crystals, and exposure times of 0.1 to 0.5 seconds per image. Diffraction data was integrated and scaled with XDS.[75] The structures were refined by using PDB ID:3IOI[35] as the starting model followed by rigid body refinement in lieu of molecular replacement. Geometry descriptions for the

inhibitors were made with Sketcher from the CCP4i suite.[76] Refinement was carried on with Refmac5,[77] model building with Coot[78] and figures were rendered with Pymol (http://www.pymol.org). A full atom anisotropic model was used for **17** and **8**-Glc, whereas TLS+ isotropic atoms were used for **8**-Gal. Data collection and refinement statistics are given in Table S1 in the Supporting Information. The atomic coordinates and structure factors have been deposited at the Protein Data Bank with the following accession codes: 4KC1 for the complex with **8**-Glc, 4KC2 with **8**-Gal, and 4KC4 with **17**.

Acknowledgements

The authors thank the Université Claude Bernard Lyon 1 and the CNRS for financial support. S.V. is grateful to financial support from the COST Action CM-1102 MultiGlycoNano. S.W. thanks the Ministère de l'Enseignement Supérieur et de la Recherche for a PhD stipend under international program. Dr. F. Albrieux, C. Duchamp, and N. Henriques are gratefully acknowledged for mass spectrometry analyses. Crystallographic studies were performed on the ID23-2 beamline at the European Synchrotron Radiation Facility (ESRF), Grenoble, France. We are grateful to DANSCATT for funding beamline access. We would like to thank Dr. R. Jørgensen and G. Batot for assistance with sample preparation and crystallographic methods and Dr. Y. Yoshimura for assistance in enzymatic assays.

[1] C. Breton, S. Fournel-Gigleux, M. M. Palcic, *Curr. Opin. Sruct. Biol.* **2012**, *22*, 540–549.
[2] L. L. Lairson, B. Henrissat, G. J. Davies, S. G. Withers, *Annu. Rev. Biochem.* **2008**, *77*, 521–555.
[3] L. F. Leloir, *Science* **1971**, *172*, 1299–1303.
[4] G. Walz, A. Aruffo, W. Kolanus, M. Bevilacqua, B. Seed, *Science* **1990**, *250*, 1132–1135.
[5] M. L. Phillips, E. Nudelman, F. C. Gaeta, M. Perez, A. K. Singhal, S. Hakomori, J. C. Paulson, *Science* **1990**, *250*, 1130–1132.
[6] P.-C. Pang, P. C. N. Chiu, C.-L. Lee, L.-Y. Chang, M. Panico, H. R. Morris, S. M. Haslam, K.-H. Khoo, G. F. Clark, W. S. B. Yeung, A. Dell, *Science* **2011**, *333*, 1761–1764.
[7] B. Nixon, Q. Lu, M. J. Wassler, C. I. Foote, M. A. Ensslin, *Cells Tissues Organs* **2001**, *168*, 46–57.
[8] J. S. Axford, *Biochim. Biophys. Acta Mol. Basis Dis.* **1999**, *1455*, 219–229.
[9] K. Furukawa, K. Matsuta, F. Takeuchi, E. Kosuge, T. Miyamoto, A. Kobata, *Int. Immunol.* **1990**, *2*, 105–112.
[10] M. Amado, R. Almeida, T. Schwientek, H. Clausen, *Biochim. Biophys. Acta Gen. Subj.* **1999**, *1473*, 35–53.
[11] I. Brockhausen, *Biochim. Biophys. Acta Gen. Subj.* **1999**, *1473*, 67–95.
[12] U. Galili, *Biochimie* **2001**, *83*, 557–563.
[13] J. A. Alfaro, R. B. Zheng, M. Persson, J. A. Letts, R. Polakowski, Y. Bai, S. N. Borisova, N. O. L. Seto, T. L. Lowary, M. M. Palcic, S. V. Evans, *J. Biol. Chem.* **2008**, *283*, 10097–10108.
[14] R. Jørgensen, L. L. Grimm, N. Sindhuwinata, T. Peters, M. M. Palcic, *Angew. Chem.* **2012**, *124*, 4247–4251; *Angew. Chem. Int. Ed.* **2012**, *51*, 4171–4175.
[15] K. Persson, H. D. Ly, M. Dieckelmann, W. W. Wakarchuk, S. G. Withers, N. C. J. Strynadka, *Nat. Struct. Mol. Biol.* **2001**, *8*, 166–175.
[16] P. Compain, O. R. Martin, *Bioorg. Med. Chem.* **2001**, *9*, 3077–3092.
[17] P. Compain, O. R. Martin, *Curr. Top. Med. Chem.* **2003**, *3*, 541–560.
[18] M. Izumi, H. Yuasa, H. Hashimoto, *Curr. Top. Med. Chem.* **2009**, *9*, 87–105.
[19] T. Kajimoto, M. Node, *Synthesis* **2009**, 3179–3210.
[20] X. Qian, M. M. Palcic *Glycosyltransferase Inhibitors in Carbohydrates in Chemistry and Biology, Vol 3*, Wiley-VCH, Weinheim, **2000**, pp. 293–312.
[21] P. van der Peet, J. E. Ralton, M. J. McConville, S. J. Williams, *PLoS ONE* **2012**, *7*, e32642.
[22] H. C. Hang, C. Yu, K. G. Ten Hagen, E. Tian, K. A. Winans, L. A. Tabak, C. R. Bertozzi, *Chem. Biol.* **2004**, *11*, 337–345.
[23] L. V. Lee, M. L. Mitchell, S.-J. Huang, V. V. Fokin, K. B. Sharpless, C.-H. Wong, *J. Am. Chem. Soc.* **2003**, *125*, 9588–9589.
[24] J. R. Brown, B. E. Crawford, J. D. Esko, *Crit. Rev. Biochem. Mol. Biol.* **2007**, *42*, 481–515.
[25] K. Descroix, G. K. Wagner, *Org. Biomol. Chem.* **2011**, *9*, 1855–1863.
[26] J. Hajduch, G. Nam, E. J. Kim, R. Froehlich, J. A. Hanover, K. L. Kirk, *Carbohydr. Res.* **2008**, *343*, 189–195.
[27] V. Kolb, F. Amann, R. R. Schmidt, M. Duszenko, *Glycoconjugate J.* **1999**, *16*, 537–544.
[28] M. S. M. Timmer, M. V. Chumillas, W. E. Donker-Koopman, J. Alerts, G. A. van der Marel, H. S. Overkleeft, J. H. van Boom, *J. Carbohydr. Chem.* **2005**, *24*, 335–351.
[29] S. Vidal, I. Bruyere, A. Malleron, C. Auge, J.-P. Praly, *Bioorg. Med. Chem.* **2006**, *14*, 7293–7301.
[30] H. C. Dorfmueller, V. S. Borodkin, D. E. Blair, S. Pathak, I. Navratilova, D. M. F. van Aalten, *Amino Acids* **2011**, *40*, 781–792.
[31] M. M. Vaghefi, R. J. Bernacki, W. J. Hennen, R. K. Robins, *J. Med. Chem.* **1987**, *30*, 1391–1399.
[32] A. Schaëfer, J. Thiem, *J. Org. Chem.* **1999**, *64*, 24–29.
[33] F. Stolz, M. Reiner, A. Blume, W. Reutter, R. R. Schmidt, *J. Org. Chem.* **2004**, *69*, 665–679.
[34] M. M. Vaghefi, R. J. Bernacki, N. K. Dalley, B. E. Wilson, R. K. Robins, *J. Med. Chem.* **1987**, *30*, 1383–1391.
[35] T. Pesnot, R. Jorgensen, M. M. Palcic, G. K. Wagner, *Nat. Chem. Biol.* **2010**, *6*, 321–323.
[36] R. Kumar, R. Nasi, M. Bhasin, N. Huan Khieu, M. Hsieh, M. Gilbert, H. Jarrell, W. Zou, H. J. Jennings, *Carbohydr. Res.* **2013**, *378*, 45–55.
[37] R. Wang, D. H. Steensma, Y. Takaoka, J. W. Yun, T. Kajimoto, C.-H. Wong, *Bioorg. Med. Chem.* **1997**, *5*, 661–672.
[38] J. C. Errey, S. S. Lee, R. P. Gibson, F. C. Martinez, C. S. Barry, P. M. J. Jung, A. C. O'Sullivan, B. G. Davis, G. J. Davies, *Angew. Chem.* **2010**, *122*, 1256–1259; *Angew. Chem. Int. Ed.* **2010**, *49*, 1234–1237.
[39] B. J. Gross, B. C. Kraybill, S. Walker, *J. Am. Chem. Soc.* **2005**, *127*, 14588–14589.
[40] J. Jiang, M. B. Lazarus, L. Pasquina, P. Sliz, S. Walker, *Nat. Chem. Biol.* **2011**, *8*, 72–77.
[41] R. Lucas, P. Balbuena, J. C. Errey, M. A. Squire, S. S. Gurcha, M. McNeil, G. S. Besra, B. G. Davis, *ChemBioChem* **2008**, *9*, 2197–2199.
[42] K. Schaefer, J. Albers, N. Sindhuwinata, T. Peters, B. Meyer, *ChemBioChem* **2012**, *13*, 443–450.
[43] K. Vembaiyan, J. A. Pearcey, M. Bhasin, T. L. Lowary, W. Zou, *Bioorg. Med. Chem.* **2011**, *19*, 58–66.
[44] K. K. Yeoh, T. D. Butters, B. L. Wilkinson, A. J. Fairbanks, *Carbohydr. Res.* **2009**, *344*, 586–591.
[45] Y. Zhang, S. Ren, D. Sun, J. Tao, *Synth. Commun.* **2010**, *40*, 328–336.
[46] L. Ballell, R. J. Young, R. A. Field, *Org. Biomol. Chem.* **2005**, *3*, 1109–1115.
[47] S. Wang, D. Lafont, J. Rahkila, B. Picod, R. Leino, S. Vidal, *Carbohydr. Res.* **2013**, *372*, 35–46.
[48] H. Chapuis, P. Strazewski, *Tetrahedron* **2006**, *62*, 12108–12115.
[49] J. Burés, M. Martin, F. Urpi, J. Vilarrasa, *J. Org. Chem.* **2009**, *74*, 2203–2206.
[50] J. Garcia, F. Urpi, J. Vilarrasa, *Tetrahedron Lett.* **1984**, *25*, 4841–4844.
[51] M. Meldal, C. W. Tornoe, *Chem. Rev.* **2008**, *108*, 2952–3015.
[52] V. V. Rostovtsev, L. G. Green, V. V. Fokin, K. B. Sharpless, *Angew. Chem.* **2002**, *114*, 2708–2711; *Angew. Chem. Int. Ed.* **2002**, *41*, 2596–2599.
[53] C. W. Tornoe, C. Christensen, M. Meldal, *J. Org. Chem.* **2002**, *67*, 3057–3064.
[54] X. Zeng, D. Coquière, A. Alenda, E. Garrier, T. Prangé, Y. Li, O. Reinaud, I. Jabin, *Chem. Eur. J.* **2006**, *12*, 6393–6402.

[55] M.-L. Milat, P. A. Zollo, P. Sinaÿ, *Carbohydr. Res.* **1982**, *100*, 263–271.
[56] R. R. Schmidt, J. Michel, *Angew. Chem.* **1980**, *92*, 763–764; *Angew. Chem. Int. Ed. Engl.* **1980**, *19*, 731–732.
[57] R. R. Schmidt, M. Stumpp, *Liebigs Ann. Chem.* **1983**, 1249–1256.
[58] H. Chen, J. Zhao, Y. Li, F. Shen, X. Li, Q. Yin, Z. Qin, X. Yan, Y. Wang, P. Zhang, J. Zhang, *Bioorg. Med. Chem. Lett.* **2011**, *21*, 574–576.
[59] M. Niemietz, L. Perkams, J. Hoffman, S. Eller, C. Unverzagt, *Chem. Commun.* **2011**, *47*, 10485–10487.
[60] M. Adinolfi, G. Barone, L. Guariniello, A. Iadonisi, *Tetrahedron Lett.* **1999**, *40*, 8439–8441.
[61] Y. Nishihara, E. Inoue, Y. Okada, K. Takagi, *Synlett* **2008**, 3041–3045.
[62] Y. Nishihara, K. Ikegashira, A. Mori, T. Hiyama, *Chem. Lett.* **1997**, *26*, 1233–1234.
[63] Y. Nishihara, S. Noyori, T. Okamoto, M. Suetsugu, M. Iwasaki, *Chem. Lett.* **2011**, *40*, 972–974.
[64] Y. Nishihara, K. Ikegashira, K. Hirabayashi, J.-i. Ando, A. Mori, T. Hiyama, *J. Org. Chem.* **2000**, *65*, 1780–1787.
[65] Y. Nishihara, E. Inoue, D. Ogawa, Y. Okada, S. Noyori, K. Takagi, *Tetrahedron Lett.* **2009**, *50*, 4643–4646.
[66] Y. Nishihara, E. Inoue, S. Noyori, D. Ogawa, Y. Okada, M. Iwasaki, K. Takagi, *Tetrahedron* **2012**, *68*, 4869–4881.
[67] T. L. Mindt, C. Schweinsberg, L. Brans, A. Hagenbach, U. Abram, D. Tourwé, E. Garcia-Garayoa, R. Schibli, *ChemMedChem* **2009**, *4*, 529–539.
[68] V. Aucagne, D. A. Leigh, *Org. Lett.* **2006**, *8*, 4505–4507.
[69] Y. Li, M. Pink, J. A. Karty, A. H. Flood, *J. Am. Chem. Soc.* **2008**, *130*, 17293–17295.
[70] www.graphpad.com
[71] N. O. L. Seto, M. M. Palcic, C. A. Compston, H. Li, D. R. Bundle, S. A. Narang, *J. Biol. Chem.* **1997**, *272*, 14133–14138.
[72] N. O. L. Seto, M. M. Palcic, O. Hindsgaul, D. R. Bundle, S. A. Narang, *Eur. J. Biochem.* **1995**, *234*, 323–328.
[73] J. R. Rich, A. Szpacenko, M. M. Palcic, D. R. Bundle, *Angew. Chem.* **2004**, *116*, 623–625; *Angew. Chem. Int. Ed.* **2004**, *43*, 613–615.
[74] K. Sujino, T. Uchiyama, O. Hindsgaul, N. O. L. Seto, W. W. Wakarchuk, M. M. Palcic, *J. Am. Chem. Soc.* **2000**, *122*, 1261–1269.
[75] W. Kabsch, *Acta Crystallogr. Sect. D* **2010**, *66*, 125–132.
[76] Collaborative Computational Project, Number 4. The CCP4 suite, programs for protein crystallography, *Acta Crystallogr. Sect. D* **1994**, *50*, 760–763.
[77] G. N. Murshudov, A. A. Vagin, E. J. Dodson, *Acta Crystallogr. Sect. D* **1997**, *53*, 240–255.
[78] P. Emsley, B. Lohkamp, W. G. Scott, K. Cowtan, *Acta Crystallogr. Sect. D* **2010**, *66*, 486–501.

Received: May 15, 2013
Revised: July 25, 2013
Published online: September 23, 2013

